Computational Study of γ-Butyrolactone and Li^+/γ-butyrolactone in Gas and Liquid Phases

Marco Masia* and Rossend Rey

Departament de Física i Enginyeria Nuclear, Universitat Politécnica de Catalunya, Campus Nord B4-B5, Barcelona 08034, Spain

Received: July 8, 2004; In Final Form: September 8, 2004

A comprehensive study of structural and dynamical properties of γ-butyrolactone (GBL) and the extent to which they are affected in the vicinity of a lithium ion, both in gas and liquid phases, is reported. The isolated GBL molecule is found to be nonplanar, with a barrier of ≈9 kJ/mol to ring inversion. As expected, the lithium ion coordinates the carbonyl oxygen with an almost collinear configuration relative to the carbon−oxygen bond but with a slight tilting toward the lactone oxygen. This configuration holds for clusters of up to four molecules and in the liquid phase as well (where a tetrahedral first solvation shell is found). A high level ab initio vibrational analysis, with a new assignment of bands has been performed, which shows substantial red and blue shifts upon lithium solvation, which decrease in a nontrivial way upon increasing the cluster size. To study the solvent effect of the vibrational spectrum, an accurate intramolecular force field has been developed, based on the concept of relaxed potential energy profiles. The inclusion of stretch and bend anharmonicity is shown to be essential in order to explain, not only the absolute value, but the sign of the shifts, particularly for the carbonyl stretching which is substantially downshifted. The shifts obtained for the rest of the bands, together with the diffusion coefficients for bulk GBL and for lithium, are in fair agreement with experimental results.

I. Introduction

γ-Butyrolactone (GBL, 4-hydroxybutyric acid gamma-lactone, Figure 1), the simplest cyclic ester, is a major chemical compound with extensive application in pharmaceuticals, pesticides and petrochemicals.[1−6] It is also known to be a building block of many natural products of biological activity, like the sesquiterpene lactones, flavor components, alkaloids, antileukemics, and pheromones.[8−11] Its biological relevance is attributed to its similarity with cyclic peptides.

Recently, GBL has become the focus of increasing technological interest for its application in lithium ion batteries (LIBs). Its physicochemical properties make it suitable to enhance LIBs capabilities (reciclability, power, etc.).[12] It is an aprotic polar solvent of moderate viscosity with a dielectric constant of 41.7 at ambient temperature, which shows a good solubilizing power for lithium salts. Contrary to other good plasticizers employed in LIBs, the liquid-phase exists over a wide range of temperatures (the melting and the boiling points are −42 and +206 °C, respectively). Takami et al.[6] have recently reported that the mixture of GBL with ethylene carbonate (EC) is a promising liquid electrolyte for thin LIBs.

Despite its importance for basic and applied areas, to our knowledge, there are no complete ab initio studies of its structure and vibrational manifold, nor any molecular dynamics (MD) simulation in the liquid phase, particularly in the vicinity of the lithium ion. The only theoretical studies to date concern molecular mechanics (MM) calculation of structures,[13−15] and ab initio computations of some partial aspects[16−20] (see below). In contrast, and probably due to the aforementioned high technological impact on LIBs, a substantial amount of experimental work has been reported for Li^+−GBL[1,2,18,21−28] and for its mixtures with other plasticizers.[6,29]

* To whom correspondence should be addressed. E-mail: marco.masia@upc.es.

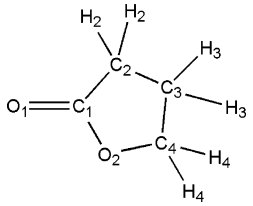

Figure 1. γ-Butyrolactone with the atom labeling used in the text (notice that hydrogens are grouped in classes).

Here we have aimed to obtain a comprehensive theoretical understanding at the molecular level: from the isolated molecule up to the solvation of the lithum ion in the liquid phase. Both ab initio and MD calculations have been used to that purpose. For the gas phase, the optimal structure and vibrational frequencies have been computed for the monomer, including a complete assignment of bands. Structure and vibrational frequencies have also been studied for clusters of Li^+, with up to four GBL molecules, as a function of solvation number. Finally, and still within the gas phase, an accurate anharmonic intramolecular force field has been developed, following a novel procedure for parametrization based on the concept of relaxed potential energy profiles along internal coordinates. Concerning the liquid state, both neat liquid GBL and Li^+ dissolved in GBL have been studied. To this end, a standard intermolecular force field has been refined, checking its goodness against counterpoise corrected potential energy profiles. Finally, a detailed study of diffusion and vibrational shifts for molecules within the first solvation shell of lithium has been performed.

The paper is organized as follows: in section II the computational details are described, section III contains the results of the ab initio calculations in the gas phase, and section IV contains those for the liquid phase. Finally, the main aspects are summarized in the conclusions section.

10.1021/jp046979i CCC: $27.50
Published on Web 10/23/2004

TABLE 1: Cartesian Coordinates for the Minimum Energy Structure, Lennard-Jones Parameters, and Charges for the Intermolecular Interaction

atom	x	y	z	σ (Å)	ϵ (kcal mol^{-1})	charge (e)
O_1	0.00000	0.00000	0.00000	2.96	0.210	−0.532
C_1	0.00000	0.00000	1.20280	3.75	0.105	0.723
C_2	1.19147	0.00000	2.15166	3.50	0.066	−0.165
O_2	−1.15362	−0.00118	1.93714	3.00	0.170	−0.432
C_3	0.57957	0.47337	3.46735	3.50	0.066	−0.059
C_4	−0.84004	−0.08158	3.34160	3.00	0.105	0.153
H_2	0.54938	1.56630	3.50044	1.80	0.030	0.069
H_2	1.09264	0.10562	4.35823	1.80	0.030	0.069
H_3	−1.59565	0.49234	3.87823	1.80	0.030	0.042
H_3	−0.88941	−1.13199	3.64882	1.80	0.030	0.042
H_4	1.55847	−1.03058	2.22354	1.80	0.030	0.045
H_4	1.99083	0.62373	1.75112	1.80	0.030	0.045

II. Computational Details

All ab initio calculations were performed with Gaussian 98.[30] Vibrational analysis and geometry optimization were performed at the MP2 level with the 6-311G basis set augmented with diffuse and polarization functions.[31] The same model chemistry has been employed for a relaxed potential energy surface scan. Because of the high memory requirements, the study of the complexes $[Li(GBL)_n]^+$ with n ranging from 1 to 4 is performed using the MP2/6-31G model chemistry.

Classical calculations were performed with an in-house MM code, together with the DL_POLY[32,33] suite. The MM code was used for the scan of the potential energy surface of a single GBL molecule using a classical intramolecular force field, and for the vibrational analysis. Finally, the DL_POLY package was used to perform the liquid-phase simulations. Data analysis (FFT, curve smoothing, and curve fitting) was performed with the commercial package Microcal Origin 6.1.[34]

III. AB Initio Calculations

A. Structure 1. *1. Single Molecule.* On the experimental side, infrared,[21,24] Raman,[24] and microwave spectra[22,23,25] of GBL have been reported. On the other hand, most of the theoretical studies correspond to MM calculations (with generic force fields) of properties such as heats of formation and minimum energy structures.[13−15,17] To our knowledge, previous ab initio calculations for GBL (using lower levels of theory) were aimed to study partial aspects such as ring inversion,[16] the effect of isotopic substitution on vibrational circular dichroism,[18] intrinsic basicities,[19] and thermal decomposition.[20] As a consequence most of the structural and vibrational measures remain to be addressed at the ab initio level.

In first place, a geometry optimization of the molecule at the MP2/6-311++G(d,p) level has been performed. The Cartesian coordinates obtained for the minimum energy structure are given in Table 1. Tables 2−4 contain the equilibrium values obtained for the internal coordinates, together with those reported in previous works (obtained experimentally,[24] with MM methods[14] or with lower level quantum chemical calculations[18]). A good agreement among all results is achieved for bond lengths and bending angles, whereas the values for some dihedral angles show somewhat larger deviations, particularly for the $O_2-C_1-C_2-C_3$ angle (to our knowledge no experimental results are available for dihedral angles).

A basic aspect to consider is that of molecular planarity. Confirming previous works,[13,14,16,25] we found that the β-carbon lies out of the plane of the remaining four ring atoms resulting in C_1 symmetry. With the assumption that the two ring puckering coordinates could be treated separately, Lopez et al.[25] demonstrated that the barrier for inversion of the GBL ring could be reliably described using a one-dimensional potential function. Indeed, a typical double well potential for inversion is obtained from a relaxed potential energy scan of the $C_2-C_3-C_4-O_2$ dihedral angle (Figure 2, see details in section III C). Microwave spectroscopy measurements[25] predict a barrier height for ring inversion of ≈8.0 kJ mol^{-1}. Our quantum chemical calculation produces a slightly higher value (≈9.0 kJ mol^{-1}), with the maximum located at 0° (i.e., a planar conformation). This conclusion agrees with the expectation of Cremer and Pople in their study on general monocyclic rings,[35] according to which a planar ring should imply a more highly strained ring angle at the carbonyl atom than a twisted conformation. Regarding other dihedrals (Table 4), our results are very similar to previous ab initio calculations[18] but show deviations of up to 8° if compared with MM results.[14]

TABLE 2: Intramolecular Force Field Parameters For Stretchings[a]

bond	k_{r_2}	k_{r_3}	k_{r_4}	r_0	MM	exp.	AI
O_1-C_1	921.20	−2225.23	3362.30	1.2028	1.211	1.239	1.180
C_1-C_2	266.95	−544.87	644.95	1.5231	1.514	1.515	1.517
C_1-O_2	331.50	−920.47	1344.25	1.3675	1.359	1.347	1.335
C_2-C_3	295.60	−573.20	633.08	1.5263	1.527	1.529	−
C_3-C_4	276.30	−561.17	627.53	1.5294	1.530	1.530	1.531
C_4-O_2	286.80	−649.33	848.48	1.4412	1.421	1.411	1.419
C_2-H_2	398.00	−812.10	1017.75	1.0930			
C_3-H_3	398.00	−812.10	1017.75	1.0930			
C_4-H_4	398.00	−812.10	1017.75	1.0930			

[a] Units: $[k_{r_i}]$ = kcal mol^{-1} Å^{-i}, $[r_0]$ = Å. Comparison of the equilibrium values with previous studies: molecular mechanics calculations (MM[14]), experiment (exp.[24]), and ab initio (AI[18]).

TABLE 3: Intramolecular Force Field Parameters for Bendings[a]

angle	$k_{\theta 2}$	$k_{\theta 3}$	θ_0	MM	exp.	AI
$O_1-C_1-C_2$	44.95	−40.10	128.5350			
$O_1-C_1-O_2$	95.20	−49.23	122.4780			
$C_1-C_2-C_3$	92.10	0.00	102.9020	103.0	102.2	
$C_2-C_3-C_4$	92.45	0.00	100.8770	101.4	99.4	
$C_3-C_4-O_2$	100.40	0.00	105.1830	106.2	105.1	105.2
$C_4-O_2-C_1$	70.95	10.07	109.8680	111.2	110.2	112.0
$O_2-C_1-C_2$	100.95	−31.54	108.9870	108.9	109.7	109.1
$C_1-C_2-H_2$	47.85	−16.43	108.9000			
$C_3-C_2-H_2$	47.85	−16.43	113.6700			
$C_2-C_3-H_3$	47.85	−16.43	112.2700			
$C_4-C_3-H_3$	47.85	−16.43	111.1200			
$C_3-C_4-H_4$	47.85	−16.43	112.9150			
$O_2-C_4-H_4$	65.10	−22.93	107.9540			
$H_2-C_2-H_2$	41.45	−21.57	108.4510			
$H_3-C_3-H_3$	41.45	−21.57	108.9570			
$H_4-C_4-H_4$	41.45	−21.57	109.6030			

[a] Units: $[k_{\theta_i}]$ = kcal mol^{-1} rad^{-i}, $[\theta_0]$ = rad. Comparison of the equilibrium values with previous studies: molecular mechanics calculations (MM[14]), experiment (exp.[24]), and ab Initio (AI[18]).

TABLE 4: Comparison of the Equilibrium Values for the Most Representative Dihedral Angles (degrees) with Previous Studies: Molecular Mechanics[a] (MM[14]) and ab Initio (AI[18]) Calculations

dihedral	ϕ_0	MM	AI
$O_1-C_1-C_2-C_3$	161.523		
$O_1-C_1-O_2-C_4$	176.531		177.391
$C_1-C_2-C_3-C_4$	31.142	29.0	
$C_1-O_2-C_4-C_3$	24.112	16.4	20.484
$O_2-C_1-C_2-C_3$	−18.664	−21.2	
$C_2-C_3-C_4-O_2$	−34.080	−28.3	
$C_2-C_1-O_2-C_4$	−3.295	3.2	−2.355

[a] The sign conventions have been adapted to the ones used here.

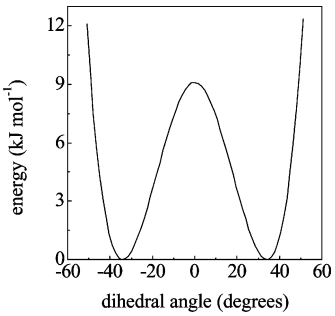

Figure 2. rPES profile along the $C_2-C_3-C_4-O_2$ dihedral angle.

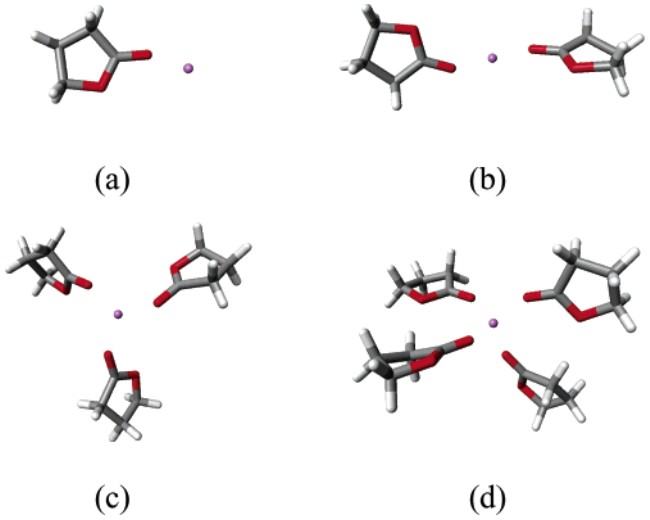

Figure 3. γ-Butyrolactone and its complexes $[Li(GBL)_n]^+$ with $1 \leq n \leq 4$. The following colors are assigned to different atomic species: red to oxygen, gray to carbon, white to hydrogen, and violet to lithium.

Some final remarks can be made on the structure: the carbonyl bond axis (O_1-C_1) is slightly tilted (3°) with respect to the bisetrix of the $C_2-C_1-O_2$ angle, which results in a distance among the two oxygens shorter than the O_1-C_2 separation. For what concerns the hydrogen atoms, differences in their distances from the carbons (~1.09 Å), or in the H−C−H bending angle (~109°) are negligible.

2. $[Li(GBL)_n]^+$ ($n = 1-4$) Clusters. In a recent study of ethylene carbonate,[36] a molecule very similar to GBL (the α-methylene group is substituted by an oxygen), we found that the interaction with lithium affects the structure causing the distortion of the molecule. A high level calculation (MP2/6-31++G(d,p)) of the complex $[Li(GBL)]^+$ has been performed to look into the most important changes in the equilibrium geometry of the molecule (Figure 3a). In the previous subsection, it was observed that the carbonyl axis of the single molecule is slightly tilted toward the lactone oxygen; this would suggest that the lithium ion might be coordinated by both oxygens if the oxygen atoms could get closer upon ion coordination. This possibility has to be discarded because both the angle among the carbonyl axis and the bisetrix of the $C_2-C_1-O_2$ angle and the O_1-O_2 distance remain fixed. On the other hand, our calculations clearly show that the lithium ion is only coordinated by O_1, but still lying out of the carbonyl axis, a muted signal of the presence of the lactone oxygen. Compared to EC, GBL seems to be slightly more rigid: coordination affects some bond lengths (mainly O_1-C_1, C_1-O_2 and C_4-O_2), whereas bending and dihedral angles are almost unaffected. A representative example is given by the change of the torsional angle $C_2-C_3-C_4-O_2$ upon coordination: when passing from the monomer to the dimer it diminishes by ~13° in EC, whereas in GBL it only varies by ~5°. To convey a clearer idea of the changes induced by the complexation, in Table 5, we report the values for the most affected internal coordinates.

Experimental results obtained with Raman spectroscopy for the liquid state suggest that the lithium ion is coordinated by four GBL molecules[37] (a coordination number that has been found both for small molecules as water and for larger ones such as EC). We studied the structure of all GBL complexes (from 1 to 4 molecules plus the lithium ion, Figure 3) with a MP2/6-31G model chemistry (the calculations for the single molecule have also been repeated at this lower level of theory, to facilitate a consistent comparison along the series). The minimum energy geometry for the two-coordinated complex has a linear arrangement with the lithium ion coordinated at opposite sides by the carbonyl oxygens, with the two GBL molecules lying on perpendicular planes. The three-coordinated complex shows a trigonal configuration with the GBL molecules slightly tilted to reduce the repulsion. The four-coordinated complex shows a tetrahedral like arrangement as the carbonyl oxygens form a dihedral angle of ~75°. Similar results for the structure of these complexes where also obtained for EC. As in that case, distortions of the molecular structure become smaller upon increasing the coordination number, most probably due to the increasing distance between lithium and the carbonyl oxygens. Again, if we compare the distortion induced in the torsional angle in EC and GBL, we notice that the GBL molecule is more rigid than EC. Finally, the angle between carbonyl axis and the vector joining the ion with the oxygen decreases from ~157° to ~140° as the coordination number increases, an aspect of interest in the analysis of liquid-phase results.

B. Vibrations. *1. Single Molecule.* In Table 6, we report the harmonic frequencies obtained from ab initio calculations, those obtained with the force field developed in this work (see section III C), the experimental measures, and, finally, the band assignment. It is known that the neglect of anharmonicity is a source of disagreement with experimental results, mainly for high frequency modes. Recently, Scott et Radom[38] published generic scaling factors for these frequencies so that ab initio results can be brought to better agreement with experiment. For MP2/6-311G(d,p) quantum chemical calculations, they proposed a scaling factor of 0.9496. Even though our model chemistry is slightly different (for the inclusion of the ++ diffuse function in the basis set), using the same factor for the highest frequencies, the corrected ab initio frequencies agree very well with experiment.

The most recent vibrational analysis is the one by McDermott,[24] who used a modified Urey−Bradley force field, with structural assumptions based on experimental measures[22,23] and previous theoretical works.[13] Fourteen modes differ from our assignment (see Table 6, bold typeface), although only a few of them can be considered to be substantial. Particularly important is that the ν_{11} mode had been assigned to the C_1-O_2 stretching, whereas we find that this stretch probably corresponds to ν_{17} (what agrees with typical results for lactones[39]). Moreover, CH_2 rocking modes had been assigned to bands for which we find C−C or O−C stretching modes and vice versa, a shuffling that can probably be explained if we notice that this zone of the spectrum is particularly crowded (7 bands in ca. 300 cm^{-1}). At lower frequencies, we find important differences for ν_{27}, ν_{28}, and ν_{30} which had been previously assigned respectively to the in-plane ring-C═O torsion, the out of plane, and the in-plane bending of the carbonyl, although here they

TABLE 5: Values for the Most Affected Coordinates by Ion Coordination Both for High and Low Level Calculations

	MP2/6-311++G(d,p)		MP2/6-31G				
	GBL	$[Li(GBL)]^+$	GBL	$[Li(GBL)]^+$	$[Li(GBL)_2]^+$	$[Li(GBL)_3]^+$	$[Li(GBL)_4]^+$
Li^+-O_1		1.786		1.778	1.831	1.900	1.934
O_1-C_1	1.203	1.233	1.240	1.267	1.261	1.255	1.253
C_1-O_2	1.367	1.315	1.417	1.353	1.364	1.378	1.383
C_1-C_2	1.523	1.505	1.535	1.519	1.521	1.523	1.525
C_2-C_3	1.526	1.531	1.548	1.555	1.554	1.552	1.551
C_3-C_4	1.529	1.527	1.551	1.550	1.550	1.550	1.551
C_4-O_2	1.441	1.471	1.499	1.537	1.529	1.522	1.515
$Li^+-O_1-C_1$		154.2		157.6	150.9	143.5	139.9
$O_1-C_1-O_2$	122.5	121.1	122.0	120.5	120.8	121.1	121.4
$O_1-C_1-C_2$	128.5	127.1	128.7	127.2	127.4	127.6	127.9
$C_2-C_3-C_4-O_2$	−34.08	−31.03	−29.2	−24.1	−24.8	−26.1	−27.7

TABLE 6: Vibrational Analysis: High Level Ab Initio, Classical, and Experimental[24] Frequencies (cm^{-1}) and Mode Assignments[a]

normal mode	GBL-G98	classical	IR	Raman	assignment	$[Li(GBL)]^+$-G98	shift
ν_1	3188.1 (3027.4)	3229.1	3000	2990	CH_2 asym. stretching	3185.8 (3025.2)	−2.3
ν_2	3183.0 (3022.6)	3224.0	3000	2990	CH_2 asym. stretching	3224.3 (3049.9)	+41.3
ν_3	3170.6 (3010.8)	3220.4	3000	2990	CH_2 asym. stretching	3195.2 (3022.3)	+24.6
ν_4	3106.4 (2949.8)	3148.9	2930	2920	CH_2 sym. stretching	3123.1 (2965.7)	+16.7
ν_5	3096.3 (2940.2)	3146.0	2930	2920	CH_2 sym. stretching	3093.3 (2937.4)	−3.0
ν_6	3090.4 (2934.6)	3144.5	2930	2920	CH_2 sym. stretching	3135.5 (2977.4)	+45.1
ν_7	1844.0 (1751.0)	1949.3	1770	1765	$C_1=O_1$ streching	1767.1 (1678.0)	−76.9
ν_8	1543.9 (1466.1)	1594.3	1487	1488	CH_2 scissoring	1543.6 (1465.8)	−0.3
ν_9	1511.5 (1435.3)	1576.9	1463	1464	CH_2 scissoring	1541.9 (1464.2)	+30.4
ν_{10}	1478.6 (1404.1)	1560.8	1425	1425	CH_2 scissoring	1469.3 (1395.2)	−9.3
ν_{11}	1417.9 (1346.4)	1521.5	1378	1378	**CH_2 wagging**	1455.5 (1382.1)	+37.6
ν_{12}	1361.6	1420.6	1318		CH_2 wagging	1378.5	+16.9
ν_{13}	1320.6	1400.7	1288		CH_2 wagging	1336.8	+16.2
ν_{14}	1285.5	1316.9	1280	1280	**CH_2 twisting**	1268.2	−17.3
ν_{15}	1232.4	1280.1	1240	1245	CH_2 twisting	1238.3	+5.9
ν_{16}	1214.0	1180.3	1200	1200	CH_2 twisting	1217.4	+3.4
ν_{17}	1179.3	1171.2	1180	1180	**C_1-O_2 stretching**	1295.0	+115.7
ν_{18}	1106.7	1079.4	1140		**CH_2 rocking**	1116.6	+9.9
ν_{19}	1087.1	1027.0	1085	1085	**O_2-C_4 stretching**	1074.8	−12.3
ν_{20}	1022.4	967.4	1038	1040	**C_2-C_3 stretching**	1017.0	−5.4
ν_{21}	961.6	926.7	994	995	**C_3-C_4 stretching**	964.0	+2.4
ν_{22}	911.4	902.6	934	933	**CH_2 rocking**	928.2	+16.8
ν_{23}	889.5	840.9	870	870	**CH_2 rocking**	901.7	+2.2
ν_{24}	817.8	747.0	805	805	ring breathing/C_2-C_1 stretching	832.3	+14.5
ν_{25}	681.5	634.1	675	678	**ring stretching**	732.3	+50.8
ν_{26}	640.5	603.7	637	638	**ring distortion**	655.0	+14.5
ν_{27}	529.4	545.8	539	540	**out of plane ring-$C_1=O_1$ torsion**	522.2	−7.2
ν_{28}	491.7	459.2	492	493	**in plane ring-$C_1=O_1$ bending**	454.5	−37.2
ν_{29}	231.3	230.3	205		ring twisting	229.7	−1.6
ν_{30}	152.5	152.4		170	**in plane ring-$C_1=O_1$ torsion**	184.4	+31.9

[a] The results for the mono-coordinated lithium complex are ordered following the assignment for the single molecule. The numbers in brackets are the high-frequency ab initio scaled values. The shifts with respect to the single molecule are given in the last column (positive sign is used for blueshifts).

are assigned to the out of plane ring-C=O torsion, the in-plane carbonyl bending and the in-plane ring-C=O torsion, respectively.

2. $[Li(GBL)_n]^+$ ($n = 1-4$) Clusters. As pointed out in subsection III A the coordination of lithium bears nonnegligible structural changes, what suggests that the strong interaction between GBL and the cation may also induce noticeable shifts of the vibrational frequencies. With high level quantum calculations (MP2/6-311++G(d,p)) substantial shifts (higher than 30 cm^{-1}) have been found for the following modes: ν_6, ν_7, ν_{11}, ν_{17}, ν_{25}, ν_{28}, and ν_{30}. Actually, these modes are associated with the most affected degrees of freedom upon ion coordination (see section III A). Table 6 contains the shifts for all modes of the mono-coordinated complex. It should be noted that a reordering of modes takes place in some cases upon coordination. It is the case, for instance, for ν_{17}, which frequency is upshifted by $\sim$115 cm^{-1}; since this large shift is not experienced by ν_{14-16}, it results in a swapping of modes.

A preliminary understanding of condensed phase effects might be obtained from the study of *n*-coordinated complexes. As it has been shown in the previous subsection, the structural changes on the GBL molecule decrease with increasing coordination number, an effect that can be expected as well for the vibrational shifts (an issue that was studied in detail for the EC molecule[36]). According to experimental results,[37] the four coordinated complex is the most likely in liquid phase. A detailed study of the shifts as a function of the coordination number (with up to four molecules) has been performed with a MP2/6-31G model chemistry. As the number *n* of coordinating molecules increases, also the number *m* of modes increases (according to $m = 3 \times (12 \times n + 1) - 6$). The majority of modes are localized on single molecules so that in a *n*-coordinated complex one can usually discern *n* frequencies that can easily be associated to a single mode (the average of these *n* frequencies is taken as the mode frequency). In some cases, there is a nonnegligible dispersion of frequencies (more than

TABLE 7: Vibrational Analysis: ab Initio Low Level Frequencies (cm^{-1}) for Single GBL and the Relative Shifts with its Lithium Complexes $[Li(GBL)_n]^+$[a]

normal mode	single GBL	$\Delta\nu$ $n=1$	$\Delta\nu$ $n=2$	$\Delta\nu$ $n=3$	$\Delta\nu$ $n=4$
ν_7	1726.9	−35.9	−21.6	−14.8	−7.9
ν_8	1587.2	−6.8	−5.3	−4.0	−3.7
ν_9	1568.4	2.0	2.2	1.7	1.5
ν_{10}	1548.6	−8.6	−6.5	−4.5	−1.0
ν_{11}	1406.4	21.9	15.7	9.6	5.8
ν_{12}	1395.3	8.1	6.6	5.2	4.3
ν_{13}	1357.7	2.1	2.7	2.7	3.8
ν_{14}	1277.5	−1.3	−2.5	−2.2	1.5
ν_{15}	1250.4	15.9	−50.7	9.6	7.8
ν_{16}	1195.6	48.6	67.9	6.1	3.4
ν_{17}	1145.3	54.6	80.8	52.6	34.0
ν_{18}	1122.9	18.6	18.5	16.9	16.6
ν_{19}	1054.4	5.5	5.0	3.9	4.1
ν_{20}	976.1	−12.4	−11.7	−11.5	−9.4
ν_{21}	942.7	4.8	2.4	−0.7	−0.9
ν_{22}	912.6	13.5	10.2	3.5	2.3
ν_{23}	877.5	19.8	20.9	18.9	12.8
ν_{24}	781.2	21.7	25.7	20.6	17.5
ν_{25}	661.8	66.6	18.3	27.2	19.1
ν_{26}	641.4	29.6	−6.6	18.7	12.0
ν_{27}	524.5	38.3	16.5	25.1	17.3
ν_{28}	473.4	44.6	2.5	38.7	20.2
ν_{29}	194.8	18.9	12.8	2.7	3.9
ν_{30}	143.7	16.9	30.0	13.9	23.2

[a] Positive and negative values of $\Delta\nu$ correspond to blue and red shifts, respectively.

10 cm^{-1}), so that the average value might not be fully informative. The carbonyl stretching for the four-coordinated complex is a relevant example, with frequencies of 1708, 1710, 1720, and 1736 cm^{-1}. As it will be shown, this behavior is probably a precursor of the broadening of the absorption band found in the liquid state, both in experiments and MD simulations (see section IV D). Obviously, a subset of modes is associated to vibrational motion of the whole cluster, and they have a complex character; most of them fall at wavenumbers lower than 150 cm^{-1}. An exception corresponds to some lithium-O═C modes which are found within the range of ring distortion vibrations; in the four-coordinated complex, there are three of them: $\omega_1 = 441.108$, $\omega_2 = 428.185$, and $\omega_3 = 421.648$ cm^{-1}, which will be discussed when the vibrational spectrum for the liquid phase is addressed.

Table 7 illustrates how the shifts become smaller when the coordination number increases. As will be shown in section IV D, the results for the four coordinated complex are rather similar to those obtained in the liquid phase. Several other features are worth noticing in the shifts experienced by GBL molecules for clusters. One would expect a monotonic variation of the shifts with the coordination number; remarkably, this is not the case for many degrees of freedom, as the shifts for the bis coordinated complex do not follow this trend (see for example ν_9, ν_{14}, ν_{15}, ν_{16}, ν_{17}, ν_{23}, ν_{24}, ν_{25}, ν_{26}, ν_{27}, ν_{28}, and ν_{30} in Table 7). Finally, the frequency shift decreases at different rates depending on the mode, it is not possible to find a simple relation for the magnitude of the shift as a function of the coordination number.

C. Intramolecular Force Field. There are indeed many intramolecular force fields available in the literature, like UFF,[40] AMBER,[41−43] MM3,[44−51] CHARMM,[52,53] OPLS,[54−59] and COMPASS.[60] They can be roughly divided into three classes: (i) generic ones with a large coverage (UFF), (ii) improved models restricted to some area of applications (e.g., biochemistry, AMBER, and CHARMM), and (iii) optimized parametrizations for condensed matter simulations. In the present work, we add to the view that, given the increased computational power, force fields tailored to each system can be developed (at least for molecules of the size of GBL) using as a source of reference data quantum mechanical results. This is the path followed for instance to parametrize very flexible force fields for transition metal complexes, where an accurate description of the quantum mechanical PES far from the minimum is needed.[61,62]

TABLE 8: Intramolecular Force Field Parameters For Dihedrals[a]

dihedral	A_n	δ	n
$O_1-C_1-C_2-C_3$	0.57	0.0	3
$O_1-C_1-O_2-C_4$	0.84	0.0	3
$C_1-C_2-C_3-C_4$	2.00	0.0	1
$C_1-C_2-C_3-C_4$	1.90	180.0	2
$C_1-O_2-C_4-C_3$	2.50	180.0	2
$C_2-C_1-O_2-C_4$	1.87	180.0	2
$O_2-C_1-C_2-C_3$	1.17	180.0	2
$O_2-C_1-C_2-C_3$	0.63	180.0	3
$O_2-C_1-C_2-C_3$	0.57	0.0	5
$C_2-C_3-C_4-O_2$	1.71	0.0	3
$C_2-C_3-C_4-O_2$	0.38	0.0	5
improper	ϕ_0	k_ϕ	
$O_1-C_1-C_2-O_2$	180.0	19.0	

[a] Units: $[A_n]$ = kcal mol^{-1}, $[\phi_0] = [\delta]$ = degrees, $[k_\phi]$ = kcal mol^{-1} rad^{-2}.

Recently,[36] we applied an efficient methodology to develop a force field from first principles and applied it to the EC molecule. The starting point is the usual expansion of the intramolecular potential in terms of internal coordinates (note that anharmonic terms are included for stretchings and bendings):

$$V(r,\theta,\phi) = \sum_{\text{bonds}} [k_{r_2}(r-r_0)^2 + k_{r_3}(r-r_0)^3 + k_{r_4}(r-r_0)^4] + \sum_{\text{angles}} [k_{\theta_2}(\theta-\theta_0)^2 + k_{\theta_3}(\theta-\theta_0)^3] + \sum_{\text{dihedrals}} A_n[1+\cos(n\phi-\delta)] + \sum_{\text{impropers}} [k_\phi(\phi-\phi_0)^2] = V_{\text{stretchings}}(r) + V_{\text{bendings}}(\theta) + V_{\text{dihedrals}}(\phi) + V_{\text{improper}}(\phi) \quad (1)$$

where r, θ, and ϕ denote respectively bond lengths, bending angles, and dihedral angles.

The method used to determine the parameters in the previous expansion makes use of the relaxed potential energy surface (rPES) concept.[63] In a rPES scan, the energy is computed along a given internal coordinate simultaneously optimizing all the unconstrained degrees of freedom, so that the minimum total energy is obtained along the chosen internal coordinate. Such a procedure can be performed both at the ab initio level and with the classical potential embodied in eq 1. Since the calculation is done for all internal coordinates, more rPES profiles are obtained than intramolecular degrees of freedom. This redundant description indirectly takes into account cross effects that are apparently neglected with the functional form used for the potential. The constants in eq 1 are obtained in an iterative way: after a first guess, the parameter set is refined until the classical rPES profiles reach a good convergence with the ab initio ones. Although for the stretching degrees of freedom few iterations are required to get a 100% convergence, for bending and torsional coordinates, the fitting procedure is slower. The resulting force field is summarized in Tables 2, 3, and 8. Figure 4 displays some examples of rPES profiles

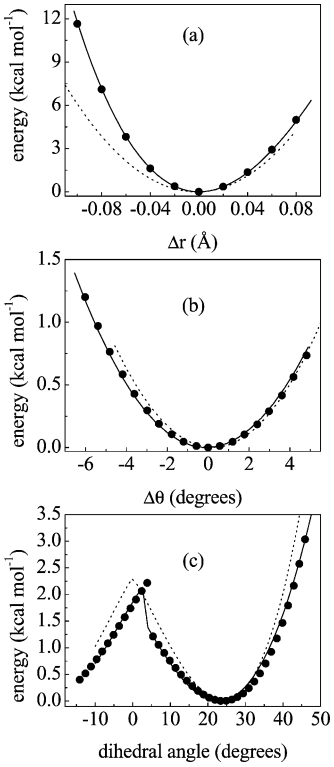

Figure 4. rPES profiles along selected internal coordinates: (a) O_1-C_1 bond, (b) $O_1-C_1-C_2$ angle, and (c) $C_3-C_4-O_2-C_1$ dihedral. Filled circles, solid line, and dotted line are used respectively for ab initio, our force field, and AMBER results.

obtained with ab initio (black circles) and classical calculations using both our (solid line) and AMBER (dotted line) force fields. Here AMBER is used as a benchmark since it probably is the most popular force field used in atomistic simulations (nevertheless we have obtained similar results with other force fields such as CHARMM, MM3, and OPLS). Our parametrization produces profiles in excellent agreement with the ab initio ones (the same degree of accord is obtained for *all* intramolecular degrees of freedom, not shown). As mentioned before, our functional form includes the anharmonic terms along stretching and bending coordinates. The quantitative importance of an anharmonic description to better address solvent induced shifts is discussed in section IV D. Panels a and b display the qualitative differences in the potential curves when anharmonicity is considered (our force field) and when not (AMBER): the ab initio profile is clearly anharmonic. Even for dihedral angles, which are obviously anharmonic in all force fields, there are noticeable differences. Panel c shows how AMBER fails to faithfully reproduce the discontinuity for the $C_3-C_4-O_2-C_1$ dihedral angle. The vibrational frequencies obtained with the model developed here are reported in Table 6, which also contains the quantum chemical results. The maximum discrepancy with ab initio results is ≈8% (≈15% with AMBER).

IV. Molecular Dynamics

A. Simulation Details. Molecular dynamics simulations of the pure liquid and of one lithium ion dissolved in liquid GBL have been performed. Table 1 contains the parameters used for the intermolecular potential. Partial charges on the atoms were obtained by fitting the electrostatic potential energy surface (obtained by ab initio MP2/6-311G++(d,p) calculations) at points selected according to the Merz−Singh−Kollman scheme,[64,65] constraining them to reproduce the total molecular dipole moment. The latter is slightly overestimated (4.708 D versus the experimental value of 4.270 D[22]), which is a desirable feature in order to balance the absence of polarization effects with fixed charge models.[65] Lennard-Jones parameters for GBL are taken from Carlson et al.[66] (with geometric average combination rules: $\sigma_{ij} = (\sigma_i \times \sigma_j)^{1/2}$, $\epsilon_{ij} = (\epsilon_i \times \epsilon_j)^{1/2}$). Indeed, with this parameter set, the diffusion coefficient is lower than the experimental one. The origin of this discrepancy lies in the radius taken for H. The value used ($\sigma = 2.5$ Å) is the one typical for hydrocarbons, whereas in GBL (and EC) the hydrogens are connected to carbon atoms that are near to electron-withdrawing groups (carbonate oxygens). This suggests that the electronic cloud for the hydrogen should be smaller. Indeed Sun et al.[67] have proposed that in the simulation of polycarbonates a value of $\sigma = 1.8$ Å should be used for hydrogen atoms which are hydrogen bonded to oxygens (it will be shown in the analysis of liquid structure that the carbonate oxygen tends to bind to hydrogens). We found that with this smaller hydrogen radius the diffusion coefficient is very near to the experimental one. Along the same line of reasoning it has been found that an optimal value for the lithium ion parameters is $\sigma = 1.3$ Å and $\epsilon = 0.191$ kcal mol^{-1}. After this parameter fine-tuning, it is important to check that the modified force field is consistent with ab initio calculations. Figure 5 displays the potential curves obtained with quantum chemical, and with the modified classical force field just described, for the Li^+-GBL dimer. The ab initio result is obtained with a counterpoise[68] correction using an MP2/6-311G(d,p) model chemistry. As can be seen, the refined parametrization performs substantially better in reproducing the interaction between GBL and the lithium ion. Obviously, the dimer potential is an approximation to the interaction in the liquid phase, where many body effects will be present, but we do not expect them to be important given the low degree of association of the neat liquid (see next section).

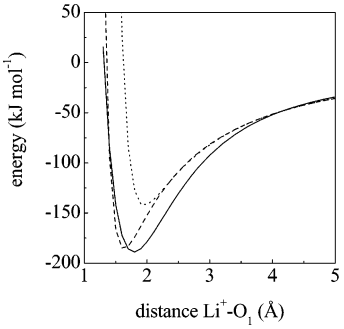

Figure 5. Potential energy for the GBL−Li^+ dimer; ab initio results (solid line), and classical results with the new (dashed line) and old (dotted line) set of Lennard-Jones parameters (see text).

All simulations were done in the NVE ensemble with a time step of 0.2 fs. The reference temperature and density were set to 298.15 K and 1.1290 g cm^{-3} (as reported in the Sigma-Aldrich catalog for the pure product). After an equilibration run of 50 ps, three productions runs of 100 ps each were completed to calculate structural and dynamical properties of the system. Two more calculations of 250 ps each were done to compute vibrational spectra. For the intramolecular interactions, we used the intramolecular force field developed in section III C and the AMBER force field for comparison. The Ewald sum was employed for electrostatic interactions.

B. Structural Properties. *1. Pure GBL.* The radial distribution function (RDF) corresponding to the molecular center of mass is displayed in panel a of Figure 6. Its overall structure is

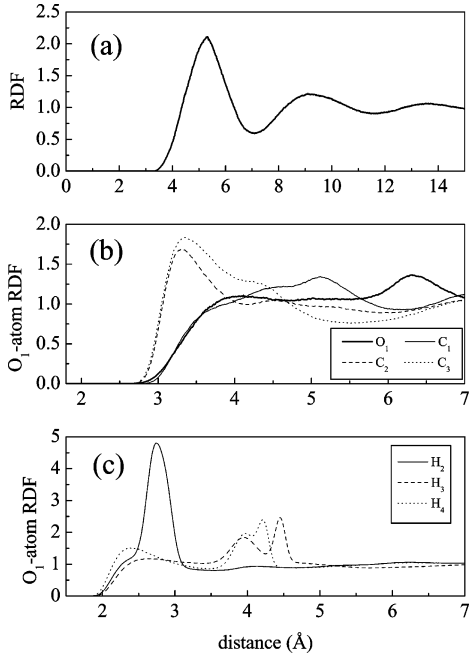

Figure 6. Molecular dynamics simulation results: (a) radial distribution function for GBL molecules' center of mass, (b) and (c) O_1-atom radial distribution functions.

very similar to that of dense simple liquids, what can be further confirmed by analysis of the solvation number N_s, defined as

$$N_s = 4\pi\rho \int_0^{r_{min}} r^2 g(r)\, dr \qquad (2)$$

where $g(r)$ denotes the RDF, ρ is the number density, and r_{min} is the first minimum of the RDF (7.1 Å). A solvation number of 12 is found, which is typical of nonassociated liquids. Although this is a signal of a low degree of order, some further insight can be obtained from the analysis of partial RDFs.

Panel b of Figure 6 displays the O_1-oxygen and O_1-carbon radial distribution functions for representative oxygen and carbon atoms. For the O_1-O_1 case, there is no first peak at 3 Å, the contact oxygen−oxygen distance, and the same result is obtained for O_1-O_2 (not shown). The corresponding RDFs are flat and start at larger separations. These features indicate that the oxygens in different molecules tend to stay away from each other, what can be explained by the strong electrostatic repulsion. Concerning the carbons, the result for O_1-C_1 are almost identical to those just discussed for the oxygen−oxygen RDFs, so that the configuration in which the carbonyl oxygen would point to C_1 of a neighboring molecule is not found. The behavior for the other carbons differs markedly, with a first peak at the contact oxygen−carbon distance (≈3.2 Å). The slight differences in peak position among different carbons correspond to their different radius (see Table 1). The results for C_4 are not shown for clarity; however, they are very similar to those for C_3 but slightly shifted to shorter distances due to the somewhat smaller carbon radius. The picture that results is one for which the carbonyl oxygen preferentially solvates the methylene groups. This is supported by the analysis of the O_1-H RDFs, with the representative examples displayed in panel c of Figure 6. Two rather different behaviors are found: for the hydrogens close to C_3 and C_4, there is a (small) first peak located at ≈2.4 Å, which corresponds to the contact O−H distance, whereas for the hydrogens close to C_2, there is a rather high peak located at a somewhat larger distance (≈2.8 Å). The latter is consistent with a bifurcated configuration in which the carbonyl oxygen of one molecule would be located midway between both hydrogens of the C_2 group (as a simple geometric calculation confirms). Such configuration is consistent with the lower height of the O_1-C_2 RDF as compared with those for O_1-C_3 or O_1-C_4: when coordinating the C_2 methylene group of one molecule, the carbonyl oxygen of the coordinating molecule tends to attach preferentially to both hydrogens rather than directly to the carbon. The peaks located at a shorter distance for the hydrogens belonging to C_3 and (to a lesser extent) C_4 are indicative of a collinear C−H···O configuration. It is also interesting to note the double peak that appears at ≈4 Å in both cases, which is consistent with the distances corresponding to the case in which the carbonyl oxygen is coordinated by both C_2 hydrogens. In conclusion, this analysis points to a substantial amount of hydrogen bonding between the carbonyl oxygen and the methylene hydrogens.

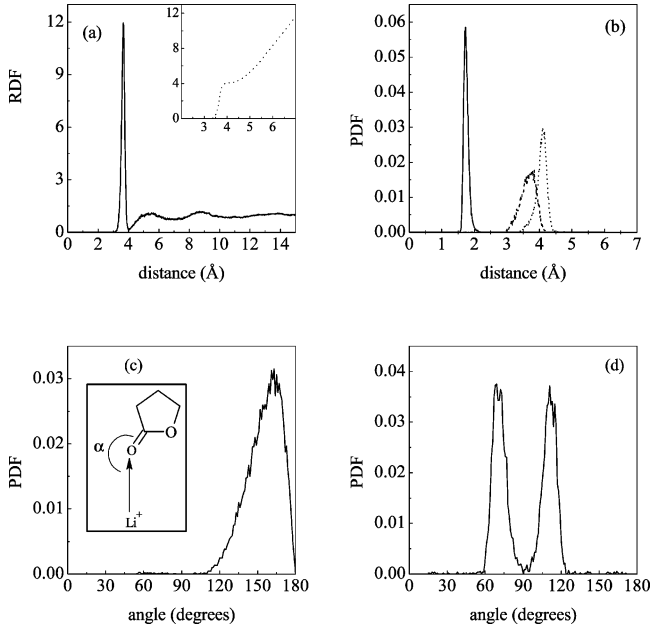

Figure 7. Structural properties of liquid GBL around lithium ion. (a) Li^+-GBL center of mass radial distribution function, and solvation number (inset). (b) Probability distribution for the distance Li^+-O_1 (solid line), Li^+-O_2 (dashed line), and Li^+-C_2 (dotted line). (c) Probability distribution for α (see inset for definition). (d) Probability distribution for the dihedral angle formed by the four carbonyl oxygens nearest to lithium.

2. GBL + Li⁺. The structural properties of the liquid around lithium are collected in Figure 7. The radial distribution function for the lithium ion is shown in panel a (the inset contains the solvation number for the first two solvation shells). We find that the solvation number is exactly four (in accord with the experimental estimation[37]) and that the radius of the first solvation shell is 4.0 Å. The structure of the complex can be compared to the one obtained with quantum chemical calculations for clusters (section III A). In panel b, the probability distribution functions for the distances Li^+-O_1, Li^+-C_2, and Li^+-O_2 are shown. The most probable distances to O_1, O_2, and C_2 are respectively 1.73, 3.74, and 4.1 Å: as in the ab initio calculations, the lithium ion is coordinated by the carbonyl oxygen and the molecule is tilted allowing the ester oxygen to lie nearer to the ion than the α-carbon. To more clearly ascertain the distortion from a linear arrangement of the $Li^+-O_1-C_1$ atoms, we computed the probability distribution for the angle (α) formed between the Li^+-O_1 and the O_1-C_1 axis (see inset in panel c for a graphical definition). A maximum exists at ∼160°, well above the result found in the gas phase for the

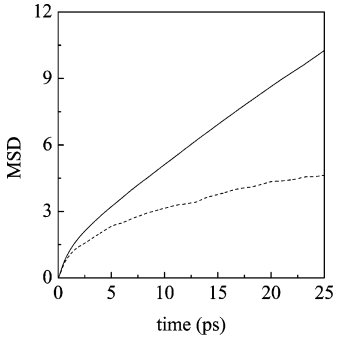

Figure 8. Molecular dynamics simulation results for the mean square displacement of GBL molecules' center of mass (solid line) and of lithium ion (dashed line).

four-coordinated complex (∼140°) and near to the value obtained for the mono-coordinated one (∼158°). Similar results were obtained for the EC case[36] and are explained by the attractive interaction with the carbonyl oxygen of second shell molecules, which tends to draw the methylene groups of first shell molecules away from the lithium ion, resulting in an angle closer to 180°. Finally, the dihedral angle formed by the carbonyl oxygens coordinating the cation (last panel) is typical of a tetrahedral structure, where the distribution is peaked at ∼71°, just 4° less than the ab initio result.

C. Diffusion. Diffusion coefficients are calculated both from the mean square displacement (MSD)

$$D_{\mathrm{MSD}} = \lim_{t\to\infty} \frac{\langle|\vec{R}(t) - \vec{R}(0)|^2\rangle}{6t} \qquad (3)$$

and from the velocity autocorrelation function (VACF)

$$D_{\mathrm{VACF}} = \frac{1}{3}\int_0^\infty \langle\vec{V}(0)\cdot\vec{V}(t)\rangle \, \mathrm{d}t \qquad (4)$$

where $\langle\cdots\rangle$ denotes the average for all time origins and all molecules' positions (velocities) of the center of mass. The actual cutoffs used in these formulas are 25 ps (for the MSD, see Figure 8) and 5 ps (for the VACF integration). The experimental value of the GBL diffusion coefficient has been recently measured by means of pulsed gradient spin−echo ^{1}H NMR,[26] and at ambient temperature, it is $\approx 0.90 \times 10^{-9}$ m^2 s^{-1}, with which our results agree satisfactorily ($D_{\mathrm{VACF}} = 0.84(\pm 0.03) \times 10^{-9}$ m^2 s^{-1} and $D_{\mathrm{MSD}} = 0.76(\pm 0.04) \times 10^{-9}$ m^2 s^{-1}). For what concerns lithium diffusion, we found very good agreement with experiment as well: Kikuko et al.[26] measured a value of $\approx 0.25 \times 10^{-9}$ m^2 s^{-1}, and we obtain $D_{\mathrm{VACF}} = 0.32(\pm 0.04) \times 10^{-9}$ m^2 s^{-1} and $D_{\mathrm{MSD}} = 0.20(\pm 0.05) \times 10^{-9}$ m^2 s^{-1}. According to Dünweg et al.,[70] due to the finite size of the simulation box, the diffusion coefficient arising from the simulation usually underestimates the value for infinite size systems. They proposed that this could be corrected by adding a constant term (χ) that depends on the simulation box dimension (L), temperature (T), and viscosity (η)

$$\chi = \frac{2.867 k_{\mathrm{B}} T}{6\pi\eta L} \qquad (5)$$

In our case, considering $\eta = 1.727$ cP,[71] we have $\chi = 0.119 \times 10^{-9}$ m^2 s^{-1}. Taking into account this correction, the diffusion coefficients for the pure liquid are even in better agreement with the experimental one.

D. Vibrational Spectrum. Vibrational spectra were obtained by fast Fourier transform (FFT) of the total dipole moment autocorrelation function computed during the simulation (including all GBL molecules or just those within the first shell of the ion, see below). According to Berens et al.[72−74] the absorption line shape is given by

$$S(\omega) = (2\pi)^{-1}\int_{-\infty}^{\infty} \mathrm{d}t \, \exp(-i\omega t)\langle\vec{M}(t)\cdot\vec{M}(0)\rangle \qquad (6)$$

where $\vec{M}$ denotes the total dipole moment. The shortness of the time series available results in a no negligible degree of noise, so that a filter is required. We used an FFT filter with 20 points for a correlation function of 100 000 points (we checked in a previous study[36] that this smoothing allows a clearer representation of the spectrum to be obtained without losing important information).

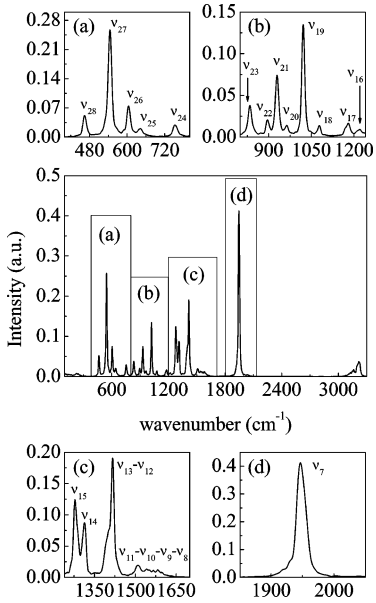

Figure 9. Middle panel: whole vibrational spectrum of pure GBL. Smaller panels: details of zones (a), (b), (c), and (d).

1. Pure GBL. The whole spectrum of liquid GBL is shown in the middle panel of Figure 9. Contrary to EC, where a number of bands did not appear in the simulated spectrum,[36] here almost all vibrational frequencies are visible. To ease the comparison with the vibrational analysis done in subsection III B, the spectrum is divided into four zones (ν_{29} and ν_{30} modes are not considered because they have a very low intensity). Panel a contains all ring modes (ν_{28} to ν_{24}); of particular intensity is the band for the out of plane ring-C═O torsion (ν_{27}). In panel b, we show all of the stretching modes for the ring bonds and the CH_2 rocking modes (ν_{23} to ν_{16}). For what concerns the remaining CH_2 modes (ν_{15} to ν_8), we can see in panel c that the scissoring and the highest frequency wagging modes (ν_{11} to ν_8) form a broad band of low intensity where the peaks cannot be easily distinguished. ν_{15} to ν_{12} modes have higher intensity and two wagging modes coalesce in a single band with a shoulder due to the ν_{13} mode. The important carbonyl stretching mode is depicted in panel d: it shows an asymmetric band which width at half-height is ∼18 cm^{-1}. Very small shifts (maximum of ∼10 cm^{-1}) of the frequencies are noticed if we compare the condensed phase and the harmonic analysis for the isolated molecule. They can be observed mainly in the CH_2 twisting and rocking modes and, of minor entity, in ring modes.

2. GBL + Li$^+$. To discern the effect of the lithium ion on the liquid phase spectrum, the dipole moment autocorrelation function was computed during the simulation only for the molecules belonging to the first solvation shell. Figure 10 shows

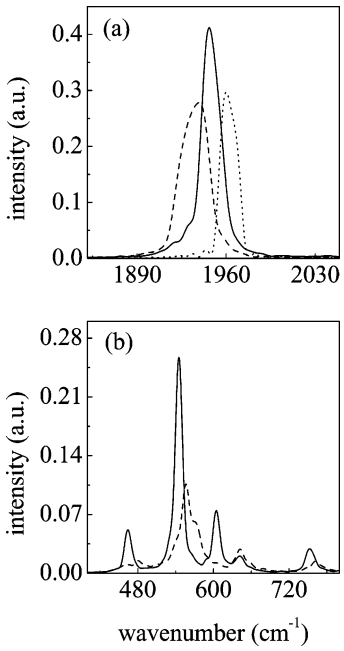

Figure 10. Comparison between the simulated vibrational spectra of bulk GBL (solid line) and first shell molecules (dashed line) for the two most representative regions, corresponding respectively to zones (d) and (a) of Figure 9. In panel a, the result with an harmonic force field is included (dotted line).

the details of what we called zones a and d for the pure solvent spectrum (previous subsection); both the pure solvent and the coordinating GBL frequencies are shown. These zones contain most of the vibrational frequencies that can be compared with experimental results: Wang et al.[27] found, with IR and Raman spectroscopy, that the most important shifts correspond to ν_7, ν_{16}, ν_{22}, ν_{24}, ν_{27}, and ν_{28}, which will be addressed in turn. It should be noted that it is not straightforward to compare with experiment because, in contrast to simulated ones, experimental spectra contain contributions of bulk and ion-coordinating molecules. Besides, experimentally there are substantial contributions from overtone and combination bands (the carbonyl stretching being a prominent example), which in contrast are muted in the simulation results.

The carbonyl stretching normal mode (ν_7) is depicted in panel a of Figure 10: upon cation coordination, we notice a redshift of $\sim$14 cm^{-1} and a broadening of the spectral band of $\sim$6 cm^{-1}. Experimentally, Wang et al. found a bigger broadening and a shoulder at lower frequencies (which might be indicative of a shift of $\sim$24 cm^{-1}). On the other hand, there is a study of Deepa et al.,[29] who found a redshift of 10 cm^{-1}. Our result thus falls midway between both experimental estimations. The same panel dramatically illustrates the effect of neglecting anharmonicity. If only the harmonic terms of the force field are considered, instead of a red shift, a blueshift is obtained. To discard that this is not a particular feature of the force field employed, similar simulations have been run using the AMBER force field (which we recall does not contain any anharmonicity for stretchings or bendings). Again the same result is obtained: upon ion coordination, the carbonyl stretching mode is upshifted to higher wavenumbers. In short, a fully harmonic force field is not able to reproduce the correct sign of the shift, what should be regarded as an important limitation of most force fields if they are to be used to interpret spectroscopic measures of solvated molecules.

For what concerns ν_{16} (CH_2 twisting mode) and ν_{22} (CH_2 rocking mode), we observed, consistently with experiment, blueshifts of respectively $\sim$27 cm^{-1} (experimental $\sim$30 cm^{-1}) and $\sim$6 cm^{-1} (experimental $\sim$10 cm^{-1}). The low intensity obtained for these bands is consistent with experiment as well, as they are only observed at high ionic concentrations. The remaining modes on which we focus are shown in panel b of Figure 10. This part of the spectrum seems to be rather sensitive to coordination. The ν_{28} mode shows a blueshift of $\sim$20 cm^{-1}. Experimentally, the presence of a new band whose intensity grows with salt concentration is observed (with a blueshift of $\sim$5 cm^{-1}). The ν_{27} mode is upshifted by $\sim$15 cm^{-1}, in line with the experimental blueshift of $\sim$8 cm^{-1}. In addition, this band shows a shoulder that might be interpreted as the contribution of lithium-GBL intermolecular modes: although in quantum chemical calculations the majority of intermolecular modes are found below 150 cm^{-1}, three of them are found in this zone of the spectrum (see subsection III B), which might explain the broad profile of the ν_{27} mode.

Finally, for what concerns ν_{24}, there is a broadening of the band whose peak is upshifted by $\sim$11 cm^{-1}; a blueshift of $\sim$22 cm^{-1} is found experimentally. Wang et al.[27] observed that the contour becomes more asymmetric as the lithium salt concentration is raised, followed by the splitting of the band at high concentrations. We should mention that in this zone of the spectrum we also observe the change in intensity of ν_{26} and ν_{25}: the former lowers substantially and the latter increases in intensity, while both are slightly upshifted (the entity of these shifts is within the order of experimental precision). Small shifts (less than 5 cm^{-1}) are also found in all low lying vibrations. Even if they are not observed experimentally, this result is consistent with our ab initio calculation on complexes as explained in section III B. We can conclude that, as a result of the strong interaction between lithium and GBL, the most affected vibrational modes are the ring distortions, the methylene rocking and twisting modes, and, obviously, the carbonyl stretching.

V. Conclusions

Concerning structural properties, it has been found in first place that the GBL monomer is nonplanar with a barrier of $\approx$9 kJ/mol for ring inversion, with the carbonyl bond axis slightly tilted toward the lactone oxygen. This structure is somewhat deformed in the presence of the lithium ion but to a lesser extent than what is found for instance in the ethylene carbonate case. As the number of molecules solvating the ion increases, the distance between the carbonyl oxygen and the ion increases as well, reducing the molecular distortion. For the important case of the four coordinated cluster, the structure is tetrahedral. In addition, the carbonyl axis is not collinear with the lithium ion, but the lactone oxygen is closer to lithium than the α-carbon. Such a configuration is maintained in the liquid phase, but with an increased tendency to a collinear configuration due to the attractive effect of second shell molecules. This attraction is explained by the analysis of radial distribution functions for neat liquid GBL: the carbonyl oxygen tends to solvate the methylene groups. Particularly, the solvation of the α-carbon differs from the two other methylene groups in that the oxygen tends to sit midway between both hydrogens.

Given that the main probes of GBL are spectroscopic, a special emphasis has been put on vibrational properties, starting with a full new assignment of bands. Substantial shifts have been found upon lithium coordination. The cases of the C$-$O stretches are particularly remarkable for the Li^+-GBL dimer: the carbonyl stretch frequency is downshifted by $\approx$77 cm^{-1}, whereas on the contrary, the C_1-O_2 stretch (which is not directly

linked to the ion) is upshifted by a larger value ($\approx$100 cm^{-1}). Ring modes are substantially affected as well. The shifts decrease upon increasing the solvation number but not necessarily in a monotonic way for all modes. This is the case for instance of the C_1-O_2 stretch, where the shift is increased for the trimer compared to the dimer, followed by a gradual decrease as the number of GBL molecules is increased. A direct comparison with experimental results is possible in the liquid phase. To this end, an intramolecular force field has been specially tailored to the GBL molecule, following a procedure founded on the concept of relaxed potential energy profiles. This new potential includes anharmonic terms for stretches (up to quartic contributions) and bends (cubic) and has been shown to be superior to conventional force fields regarding potential profiles and harmonic frequencies for the monomer. More importantly, the analysis of the carbonyl stretch in the liquid phase has illustrated how the neglect of anharmonic contributions results in a wrong sign for the predicted shift. This is a critical feature to take into consideration if one wants to use generic force fields to theoretically interpret spectroscopic measures. Finally, the calculation of the spectrum for the molecules belonging to the first shell produces results which are in fair agreement with experimental shifts. This has allowed several shoulders and/or broadenings appearing in experimental spectra to be interpreted as being due to lithium induced shifts on first shell molecules.

Acknowledgment. This work was supported by EC TMR network HPRN-CT-2000-19 ("Solvation Dynamics and Ionic Mobility in Conventional and Polymer Solvents") and MCYT project BFM2001-2077.

References and Notes

(1) Zhu, Y.-L.; Xiang, H.-W.; Wu, G.-S.; Bai, L.; Li Y.-W. *Chem. Commun.* **2002**, *3*, 254.

(2) Tarvainen, M.; Sutinen, R.; Somppi, M.; Paronen, P. *Poso A. Pharm. Res.* **2001**, *18* (12), 1760.

(3) Herrmann, U.; Eming, G. *Chem. Eng. Technol*. **1998**, *21*, 285.

(4) Harris, N.; Tuck, M. W. *Hydrocarbon Process.* **1990**, *69*, 79.

(5) Banker, G. S. *J. Pharm. Sci.* **1966**, *55*, 81.

(6) Takami, N.; Sekino, M.; Ohsaki, T.; Kanda, M.; Yamamoto, M. *J. Power Sources* **2001**, *97*−*98*, 677.

(7) Vose, J.; Tighe, T.; Schwartz, M.; Buel, E. J. *Forensic Sci.* **2001**, *46* (5), 1164.

(8) Hoffmann, H. M. R.; Rabe, J. *Angew. Chem., Int. Ed. Engl.* **1985**, *24*, 94.

(9) Koch, S. S. C.; Chamberlin, A. R. *J. Org. Chem.* **1993**, *58*, 2725.

(10) Brown, H. C.; Kulkarni, S. V.; Racherla, V. S. *J. Org. Chem.* **1994**, *59*, 365.

(11) Donate, P. M.; Frederico, D.; Da Silva, R.; Constantino, M. G.; Del Ponte, G.; Bonatto, P. S. *Tetrahedron Asym.* **2003**, *14*, 3253.

(12) Chagnes, A.; Carré B.; Willmann P.; Dedryvére R.; Gonbeau D.; Lemordant, D. *J. Electrochem. Soc.* **2003**, 150 (9), A1255.

(13) Allinger, N. L.; Chang, S. H. M. *Tetrahedron* **1977**, *33*, 1561.

(14) Allinger, N. L. *Pure Appl. Chem.* **1982**, *54* (12), 2515.

(15) Lii, J. H. *J. Phys. Chem. A* **2002**, *106*, 8667.

(16) Esposti, A. D.; Alonso, J. L.; Cervellati, R.; Lister, D. G.; Lopez, J. C.; Palmieri, P. *J. Chem. Soc., Faraday Trans.* **1990**, *86*, 459.

(17) Allinger, N. L.; Schmitz, L. R.; Motoc, I.; Bender, C.; Labanowski, J. K. *J. Comput. Chem.* **1992**, *13* (7), 838.

(18) Malon, P.; Mickley, L. J.; Sluis, K. M.; Tam, C. N.; Keiderling, T. A.; Kamath, S.; Uang, J.; Chickos, J. S. *J. Phys. Chem.* **1992**, *96*, 10139.

(19) Bouchoux, G.; Leblanc, D.; Mé, O.; Yáñez, M. *J. Org. Chem.* **1997**, *62*, 8439.

(20) Li, Z.-H.; Wang, W.-N.; Fan, K.-N.; Wong, M. W.; Huang, H.-H.; Huang, W. *Chem. Phys. Lett.* **1999**, *305*, 474.

(21) Durig, J. R.; Coulter, G. L.; Wertz, D. M. *J. Mol. Spectrosc.* **1968**, *27*, 285.

(22) Durig, J. R.; Li, Y. S.; Tong, C. C. *J. Mol. Struct.* **1973**, *18*, 269.

(23) Legon, A. C. *Chem. Commun.* **1970**, 838.

(24) McDermott, P. *J. Phys. Chem.* **1986**, *90*, 2569.

(25) Lopez, J. C.; Alonso, J. L.; Cervellati, R.; Esposti, A. D.; Lister, D. G.; Palmieri, P. *J. Chem. Soc., Faraday Trans.* **1990**, *86*, 453.

(26) Hayamizu, K.; Aihara, Y.; Arai, S.; Martinez, C. G. *J. Phys. Chem. B* **1999**, *103*, 519.

(27) Wang, J.; Xuan, X.; Lu, J.; Pei, N.; Mo, Y. Z. *Phys. Chem.* **2001**, *215*, 437.

(28) Mandal, S. K.; Amin, A. R.; Crowe, W. E. *J. Am. Chem. Soc.* **2001**, *123*, 6457.

(29) Deepa, M.; Sharma, N.; Varshney, P.; Agnihotry, S. A.; Chandra, R. *Ionics* **2000**, *6*, 408.

(30) Frisch, M. J.; Trucks, G. W.; Schlegel, H. B.; Scuseria, G. E.; Robb, M. A.; Cheeseman, J. R.; Zakrzewski, V. G.; Montgomery, J. A., Jr.; Stratmann, R. E.; Burant, J. C.; Dapprich, S.; Millam, J. M.; Daniels, A. D.; Kudin, K. N.; Strain, M. C.; Farkas, O.; Tomasi, J.; Barone, V.; Cossi, M.; Cammi, R.; Mennucci, B.; Pomelli, C.; Adamo, C.; Clifford, S.; Ochterski, J.; Petersson, G. A.; Ayala, P. Y.; Cui, Q.; Morokuma, K.; Malick, D. K.; Rabuck, A. D.; Raghavachari, K.; Foresman, J. B.; Cioslowski, J.; Ortiz, J. V.; Stefanov, B. B.; Liu, G.; Liashenko, A.; Piskorz, P.; Komaromi, I.; Gomperts, R.; Martin, R. L.; Fox, D. J.; Keith, T.; Al-Laham, M. A.; Peng, C. Y.; Nanayakkara, A.; Gonzalez, C.; Challacombe, M.; Gill, P. M. W.; Johnson, B. G.; Chen, W.; Wong, M. W.; Andres, J. L.; Head-Gordon, M.; Replogle, E. S.; Pople, J. A. *Gaussian 98*, revision A.11.2; Gaussian, Inc.: Pittsburgh, PA, 1998.

(31) Frisch, M. J.; Pople, J. A.; Binkley, J. S. *J. Chem. Phys.* **1984**, *80*, 3265.

(32) DL_POLY is a package of molecular simulation routines written by W. Smith and T. R. Forester, copyright The Council For The Central Laboratory Of The Research Council, Daresbury Laboratory at Daresbury, Nr. Warrington, 1996.

(33) http://www.cse.clrc.ac.uk/msi/software/DL_POLY/.

(34) http://www.originlab.com.

(35) Cremer, D.; Pople, J. A. *J. Am. Chem. Soc.* **1975**, *97*, 1354.

(36) Masia, M.; Probst, M.; Rey, R. *J. Phys. Chem. B* **2004**, *108*, 2016.

(37) Caillon-Caravanier, M.; Bosser, G. Claude-Montigny, B.; Lemordant, D. *J. Electrochem. Soc.* **2002**, *149*, E340.

(38) Scott, A. P.; Radom, L. *J. Phys. Chem.* **1996**, *100*, 16502.

(39) Pretsch, E.; Clerk, T.; Seibl, J.; Simon, W. *Tablas para la determinación estructural por metodós espectroscopicos*; Springer-Werlag: New York, 1998.

(40) Rappé, A. K.; Casewit, C. J.; Colwell, K. S.; Goddard, W. A., III; Skiff, W. M. *J. Am. Chem. Soc.* **1992**, *114*, 10024.

(41) Weiner, S. J.; Kollman, P. A.; Nguyen, D. T.; Case, D. A. *J. Comput. Chem.* **1986**, *7*, 230.

(42) Cornell, W. D.; Cieplak, P.; Bayly, C. I.; Gould, I. R.; Merz, K. M.; Ferguson, D. M.; Spellmeyer, D. C.; Fox, T.; Caldwell, J. W.; Kollman, P. A. *J. Am. Chem. Soc.* **1995**, *117*, 5179.

(43) http://amber.scripps.edu/.

(44) Allinger, N. L.; Yuh, Y. H.; Lii, J.-H. *J. Am. Chem. Soc.* **1989**, *111*, 8551.

(45) Lii, J.-H.; Allinger, N. L. *J. Am. Chem. Soc.* **1989**, *111*, 8566.

(46) Lii, J.-H.; Allinger, N. L. *J. Am. Chem. Soc.* **1989**, *111*, 8576.

(47) Allinger, N. L.; Geise, H. J.; Pyckhout, W.; Paquette, L. A.; Gallucci, J. C. *J. Am. Chem. Soc.* **1989**, *111*, 1106.

(48) Allinger, N. L.; Li, F.; Yan, L. *J. Comput. Chem.* **1990**, *11*, 848.

(49) Allinger, N. L.; Li F.; Yan, L.; Tai, J. C. *J. Comput. Chem.* **1990**, *11*, 868.

(50) Lii, J.-H.; Allinger, N. L. *J. Phys. Org. Chem.* **1994**, *7*, 591.

(51) Lii, J.-H.; Allinger, N. L. *J. Comput. Chem.* **1998**, *19*, 1001.

(52) MacKerrell, A. D., Jr.; Bashford, D.; Bellot, M.; Dunbrack, R. L., Jr.; Evanseck, J. D.; Field, M. J.; Fisher, S.; Gao, J.; Guo, H.; Ha, S.; Joseph-McCarthy, D.; Kuchnir, L.; Kuczera, K.; Lau, F. T. K.; Mattos, C.; Michnick, S.; Ngo, T.; Nguyen, D. T.; Prodhom, B.; Reiher, W. E., III; Roux, B.; Schlenkrich, M.; Smith, J. C.; Stote, R.; Straub, J.; Watanabe, M.; Wiórkiewicz-Kuczera, J.; Yin, D.; Karplus, M. *J. Phys. Chem. B* **1998**, *102*, 3586.

(53) Foloppe, N.; MacKerell, A. D., Jr. *J. Comput. Chem.* **2000**, *21*, 86.

(54) Jorgensen, W. L.; Maxwell, D. S.; Tirado-Rives, J. *J. Am. Chem. Soc.* **1996**, *117*, 11225.

(55) Maxwell, D. S.; Tirado-Rives, J.; Jorgensen, W. L. *J. Comput. Chem.* **1995**, *16*, 984.

(56) Jorgensen, W. L.; McDonald, N. A. *J. Mol. Struct. (THEOCHEM)* **1998**, *424*, 145.

(57) McDonald, N. A.; Jorgensen, W. L. *J. Phys. Chem. B* **1998**, *102*, 8049.

(58) Rizzo, R. C.; Jorgensen, W. L. *J. Am. Chem. Soc.* **1999**, *121*, 4827.

(59) Price, M. L. P.; Ostrovsky, D.; Jorgensen, W. L. *J. Comput. Chem.* **2001**, *22*, 1340.

(60) Sun, H. *J. Phys. Chem. B* **1998**, *102*, 7338.

(61) Villa, A.; Cosentino, U.; Pitea, D.; Moro, G.; Maiocchi, A. *J. Phys. Chem. A* **2000**, *104*, 3421.

(62) Norrby, P.-O.; Brandt, P. *Coord. Chem. Rev.* **2001**, *212*, 79.

(63) Foresman, J. B.; Frisch, Æ. *Exploring Chemistry with Electronic Structure Methods*, 2nd ed.; Gaussian, Inc.: Pittsburgh, PA, 1996.
(64) Singh, U. C.; Kollman, P. A. *J. Comput. Chem.* **1984**, *5*, 129.
(65) Besler, B. H.; Merz, K. M., Jr.; Kollman, P. A. *J. Comput. Chem.* **1990**, *11*, 431.
(66) Carlson, H. A.; Nguyen, T. B.; Orozco, M.; Jorgensen, W. L. *J. Comput. Chem.* **1993**, *14* (10), 1240.
(67) Sun, H.; Mumby, S. J.; Maple, J. R.; Hagler, A. T. *J. Am. Chem. Soc.* **1994**, *116*, 2978.
(68) van Duijneveldt, F. B.; van Duijneveldt-van de Rijdt, J. G. C. M.; van Lenthe, J. H. *Chem. Rev.* **1994**, *94*, 1873.
(69) Soetens, J. C.; Millot, C.; Maigret, B.; Bakó, J. *Mol. Liq.* **2001**, *92*, 201.
(70) Dünweg, B.; Kremer, K. *J. Chem. Phys.* **1993**, *99*, 6983.
(71) Ue, M. *J. Electrochem. Soc.* **1994**, *141*, 3336.
(72) Berens, P. H.; Wilson, K. R. *J. Chem. Phys.* **1981**, *74* (9), 4872.
(73) Berens, P. H.; White, S. R.; Wilson, K. R. *J. Chem. Phys.* **1981**, *75* (2), 515.
(74) Berens, P. H.; Mackay, D. H. J.; White, G. M.; Wilson, K. R. *J. Chem. Phys.* **1983**, *79* (5), 2375.